

# Water resource and ecotone transformation in coastal ecosystems

Joseph Park<sup>a,b,\*</sup>, Jed Redwine<sup>a,c</sup>, Troy Hill<sup>a,b</sup>, Kevin Kotun<sup>d</sup>

<sup>a</sup>*Department of Interior South Florida Natural Resources Center*

<sup>b</sup>*Physical Resources*

<sup>c</sup>*Science Communication*

<sup>d</sup>*U.S. Geological Survey*

---

## Abstract

Mangrove marshes are a significant global ecosystem, finely-tuned to contemporary sea level. As sea level rises the mangrove-to-freshwater ecotone reflects underlying groundwater salinity indicating the transformation of freshwater resources into saltwater unsuitable for consumption or agriculture. Hydrological numerical models can predict this dynamic given sufficient environmental detail, however, detailed data is often lacking. Alternatively, agent-based models can predict landscape vegetation changes and the associated fresh-to-saline water transformation based only on landscape surface features. We apply such a model to the southern tip of the Florida peninsula at the nexus of a metropolis and World Heritage wildlife preserve: the Florida Everglades, to predict ecotone dynamics and aquifer water resources in response to warming climate and rising sea level. The model is based on species-specific behaviors for freshwater grasses and salt-tolerant red mangroves with relevance to global mangrove ecosystems.

*Keywords:* Freshwater Resource, Mangrove Ecotone, Sea level rise

---

## 1. Introduction

As climate warms and sea level rises, low-lying coastal ecosystems are among the first to transform with potential for large shifts in ecotones and associated ecosystem services such as sustenance of freshwater resources.

---

\*Corresponding author

Email address: Joseph\_Park@nps.gov (Joseph Park)

These coastal ecotone dynamics reflect landscape changes from the adaptation of terrestrial, estuarine and marine ecosystems in response to perpetual and nonstationary environmental dynamics, and are expressed through a web of complex interactions and feedbacks between biota and environment. Given the inherent nonlinearity and interdependence in these dynamics, one would expect that linear systems analysis may provide unsatisfying results (DeAngelis and Yurek, 2015). As noted by Jiang et al. (2016): “While habitat transitions can be abrupt, modeling the specific drivers of abrupt change between halophytic and glycophytic vegetation is not a simple task. Correlative studies, which dominate the literature, are unlikely to establish ultimate causation for habitat shifts, and do not generate strong predictive capacity for coastal land managers”.

Traditional methods to assess these impacts rely on equation-based models where physical and biological responses are specified with mathematical expressions and/or probabilistic descriptions and interactions (Jorgensen, 1996). Such numerical models have been instrumental in the advancement of our knowledge of coastal systems, however, the expression of emergent behaviors predicated on nonlinear feedbacks can be problematic in the implementation of equation-based models.

Specific to the nexus of eco-hydrological models, Sivapalan (2018) noted difficulties in accurately quantifying the spatial heterogeneity needed to inform equation-based models, thereby complicating the expression of closure relations at scales of interest. Further, he suggested “instead of specifying exact details of the heterogeneity in our models, we can replace it (without loss of information) with the ecosystem function that they perform.” This perspective aligns with the Earth systems science approach (NASA, 1986) relying on integrative co-evolutionary interactions *in-lieu* of a physical, reductionist approach.

One such alternative is agent-based modeling, where behaviors and feedbacks at the core of the model naturally accommodate nonlinearity and emergence (Grimm, 2005). Here, we assess coastal ecotone dynamics with an agent-based model, relying on vegetative transformations in response to sea level driven porewater salinity as a marker for groundwater changes from fresh to saline. Quantification of these changes, both the landscape transformation from freshwater dominated marshes to saltwater dominated estuaries, and the associated changes in freshwater resources are fundamental to the future of inhabited and natural coastal ecosystems.

As an exemplar, we consider the southern tip of the Florida peninsula which is home to both a large metropolitan area and the Everglades (figure 1). The relationship is symbiotic as the Everglades protects and sustains

45 freshwater resources for the natural and urban communities, while concerned  
46 citizens and governments are dedicated to preservation and protection of its  
47 natural resources. Not only are the Everglades home to spacious freshwater  
48 marshes and hardwood hammocks, it includes the largest contiguous fresh–  
49 to–saltwater mangrove ecosystem in North America. Such coastal freshwa-  
50 ter/mangrove marsh ecosystems are a prominent feature around the globe,  
51 with importance as atmospheric carbon sinks, proliferent marine nurseries,  
52 and bellwethers of coastal transformation.

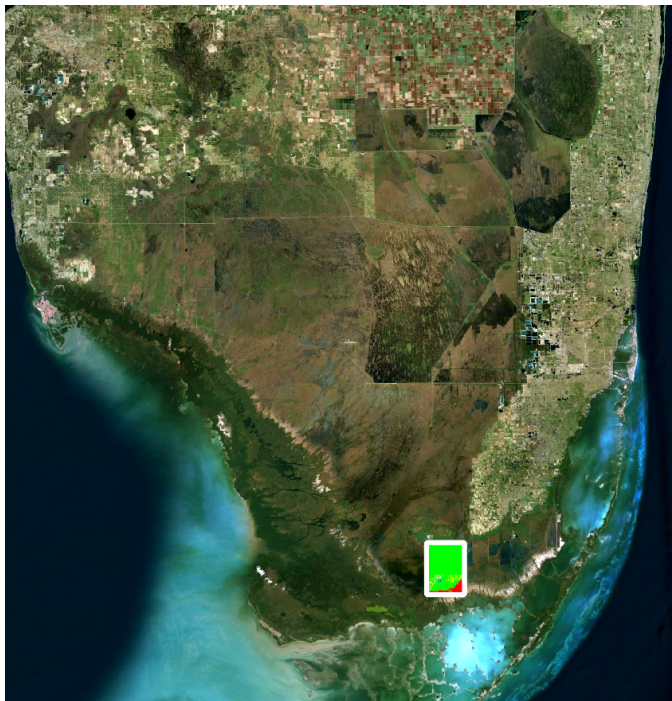


Figure 1: Southern Florida. The east coast is a metropolis of 6.7 million with the South–Dade agricultural area along the southern and western edges. The south central and southwest areas contain the Everglades and Big Cypress National Preserve. The north central area is agricultural and rural. The model domain is shown by the box in the lower center with dimensions 10.2 km x 14.1 km. Dimensions of the overall image are 180 km x 190 km.

53 **2. Materials and methods**

54 *2.1. Analysis Domain and Data*

55 We estimate the change in vegetation coverage and aquifer freshwater  
56 volume under a 14,382 hectare domain spanning a mangrove/freshwater eco-

57 tone from 2015 through 2100 in response to a low and high sea level rise  
58 trajectory. Figure 2 shows the model domain with a false color overlay of  
59 vegetation in 2015 along the southern peninsula.

60 Data inputs consist of landscape vegetation coverage obtained from a  
61 synthesis of field observations and aerial photography (Ruiz et al., 2017),  
62 marsh water levels from the Everglades Depth Estimation Network (EDEN)  
63 (USGS, 2015), land surface elevations (Fennema et al., 2015), and sea level  
64 rise trajectories (Park et al., 2017). A general description of the modelling  
65 framework is provided in the following sections, with a detailed descrip-  
66 tion following the ODD (Overview, Design concepts, and Details) protocol  
67 (Grimm et al. , 2010) in Appendix A.

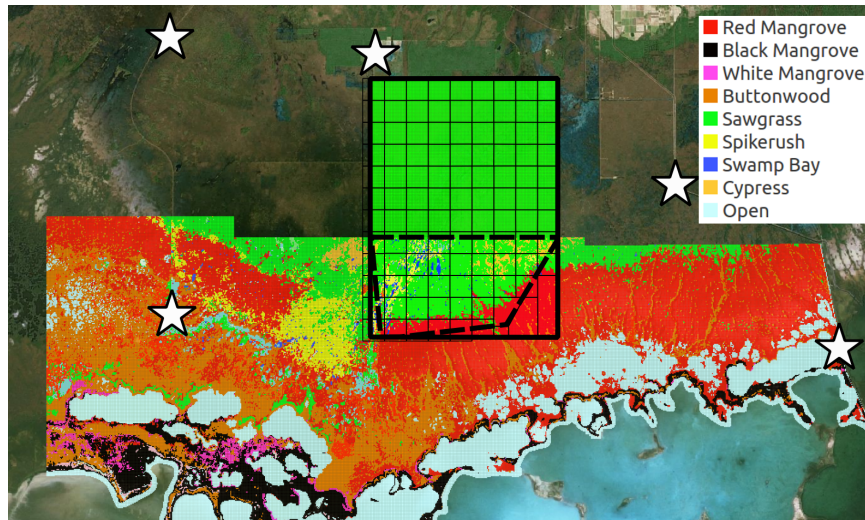


Figure 2: Southern coastal Everglades false color vegetation map. Dashed polygon shows the calibration model domain, rectangle, the future projection domain. The grid defines cells where distinct hydrologic timeseries are applied. Stars indicate locations of wells to estimate aquifer thickness.

68 *2.2. Model Framework*

69 Agent-based modeling can be viewed as an evolution of cellular au-  
70 tomata (Schiff, 2011), finding good success in the analysis of ecosystem  
71 complexity and interactions (Grimm, 2005). Agent-based models consist  
72 of dynamically interacting agents operating in a decentralized, intercon-  
73 nected paradigm accommodating complexity and emergence. NetLogo is  
74 a programmable modeling environment designed to simulate complex phe-

75 nomena in an agent-based framework (Wilensky, 1999), and is the modeling  
76 platform we employ.

77 NetLogo distinguishes four types of agents: Patches, Turtles, Links, and  
78 Observers. Patches represent the world in a grid of cells. Turtles represent  
79 agents that operate in the world, interacting with patches and each other.  
80 Links provide connections between agents. Observers allow interaction be-  
81 tween agents within, and external to the model domain. Our model defines  
82 agents for the dominant vegetation species (turtles), agents for the landscape  
83 cells (patches), and interactions between agents and the environment.

84 NetLogo programs conventionally contain **setup** and **go** procedures, the  
85 latter being executed in a loop sequencing through agents. Our **setup** pro-  
86 cedure loads the timeseries input data, loads GIS shapefiles representing the  
87 vegetation map and timeseries mappings, initializes patches with data from  
88 the GIS layers, and sprouts turtles on the patches according to the GIS  
89 vegetation map species for each cell. The **go** procedure iteratively calls the  
90 vegetation agents to assess their vitality, followed by the **propagation** pro-  
91 cedure governing species succession in response to environmental feedbacks.

### 92 2.2.1. Vitality behaviors

93 A typical vegetation agent assesses whether the vegetation on a par-  
94 ticular patch has been stressed enough to die. For example, *Cladium ja-*  
95 *maicense* (sawgrass) contains assessments of water depth and porewater  
96 salinity thresholds and durations. Agent vitality behaviors are detailed in  
97 Appendix A.4.3.

### 98 2.2.2. Succession behaviors

99 The **propagation** procedure queries each patch devoid of live vegeta-  
100 tion, assessing surrounding patches to identify neighboring species. If en-  
101 vironmental conditions are conducive for a neighboring species, the species  
102 can establish on the vacant patch according to a fitness function shown in  
103 figure 3. Note that the fitness function is only used to determine vegetation  
104 succession, not vitality.

105 First, a list of vegetation species on the surrounding (8) patches is ob-  
106 tained. A cumulative fitness score is computed for each species by summing  
107 the individual fitness scores on a per-species basis. The species with highest  
108 cumulative fitness is selected for propagation. However, whether propaga-  
109 tion actually occurs is determined by comparison of the species propaga-  
110 tion success threshold (i.e. `mangrove-success`, a user-defined parameter)  
111 against a randomly selected percentile of a uniform distribution. If succes-

112 sion fails on a particular timestep, there is no penalty on following timesteps,  
113 the propagation is run as usual.

114 Succession behavior rules are detailed in Appendix A.4.3 with water  
115 depth and hydroperiod thresholds shown in table A.4, and succession prob-  
116 abilities listed in table A.5. Threshold and model parameters values are  
117 listed in table B.11 of Appendix B.

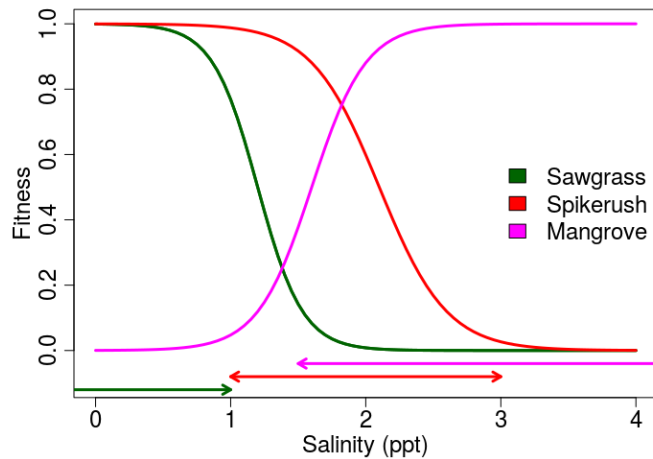


Figure 3: Succession fitness functions for the three dominant species. Horizontal arrows indicate the range of salinities observed by Ross et al. (2000).

### 118 2.2.3. Porewater salinity

119 The primary ecotone driver from freshwater to salt-tolerant plants is root  
120 zone porewater salinity. In the model this is driven by the relative elevation  
121 of mean sea level and freshwater depth on the vegetation patch. Since there  
122 is a coastal ridge along the northern shore of Florida Bay serving to buffer  
123 ocean and estuarine water from the interior, and, since freshwater in the  
124 marsh suppresses subterranean saline water in the root zone as expressed by  
125 the Ghyben–Herzburg principle, there are two model parameters to calibrate  
126 these effects: `msl-offset` and `depth-no-porewater` (see table B.11 and  
127 figure B.13).

128 All patches are initialized to porewater salinity of zero, and have a maxi-  
129 mum porewater salinity of 3. This is sufficient since the maximal glycophytic  
130 vegetation tolerance is 2 ppt (table B.11). Patch porewater salinity is then  
131 determined by progressive accumulation of porewater salinity for patches  
132 with elevation below mean sea level and no standing freshwater.

133 Procedurally, all patches with an elevation below mean sea level mi-  
134 nus the `msl-offset` parameter are selected. If these patches have a fresh  
135 water depth less than `depth-no-porewater`, then their porewater salin-  
136 ity is incremented by 1 ppt. If the fresh water depth is greater than  
137 `depth-no-porewater`, the porewater salinity is reset to zero.

### 138 2.3. Vegetation Map

139 As a component of the Comprehensive Everglades Restoration Plan  
140 (CERP), the Department of Interior conducts an extensive vegetation map-  
141 ping project. The vegetation assessment assigns a landscape characteriza-  
142 tion code, the *vegetation code*, to 50 m x 50 m patches throughout a region.  
143 Vegetation codes derive from a tree of descriptors starting with one of seven  
144 overall landscape types, for example Shrubland (S), with additional code  
145 elements providing increasing levels of landscape and ecosystem specificity  
146 as in Red Mangrove dominant Shrubland (SMr).

147 Since our model is driven by species behaviors, we assign the dominant  
148 species for each landscape code to each of the 50 x 50 m patches. For  
149 example, even though a Red Mangrove dominant Shrubland (SMr) may  
150 contain other species, the model considers such a patch to be uniformly  
151 populated with Red Mangrove. Figure 2 shows the southern coastal region  
152 vegetation map in Everglades National Park with false color overlay (Ruiz  
153 et al., 2017).

### 154 2.4. Hydrological Data

155 Hydrologic data are informed through the NetLogo `time` extension, with  
156 daily mean water levels provided as timeseries input to patch agents. The  
157 link between timeseries and patches is specified in a GIS layer corresponding  
158 to the grid shown in figure 2. Each model grid cell correspond to 3 x 3 grid  
159 blocks from the Everglades Depth Estimation Network (EDEN) (USGS,  
160 2015), with the daily water level extracted from the center EDEN cell of the  
161 3 x 3 block.

162 EDEN observed data are available from 1990 through 2017. Since the  
163 calibration model period of record is 1973 through 2015, and the projection  
164 model period of record 2015 through 2100, data extrapolation is needed. To  
165 model data from 1973 through 1990, we take advantage of strong correlations  
166 between marsh water levels across the model domain ( $R^2 = 0.89 \pm 0.09$ ) and  
167 estimate missing data with linear regressions from each cell to a long term  
168 hydrologic station (P-37) in the central Everglades containing data back to  
169 1973.

170        Projection model data also leverage strong temporospatial correlations  
171        to create future projections of stage. First, we compute a single timeseries of  
172        daily mean water level across all cells over the observational record (1990–  
173        2017) to create a reference timeseries. Second, we compute empirical cu-  
174        mulative distribution functions for each day of the year (year-day, 1-365)  
175        over all years of the reference timeseries. Third, we compute linear regres-  
176        sions between the timeseries of each grid cell (1990–2017) and the reference  
177        ( $R^2 = 0.95 \pm 0.05$ ). These correlation coefficients will be used to model grid  
178        cell water levels from a future projection of the reference timeseries.

179        Next, the reference timeseries is projected forward in time by sampling  
180        from the empirical distribution at the corresponding projected year-day with  
181        a Gaussian kernel. Specifically, for a projected year-day, say the first day  
182        of the year, the projected value is sampled from the empirical distribution  
183        for the first day of the year at a random percentile selected from a normal  
184        distribution to produce a projected reference timeseries (2015–2100).

185        To generate projected timeseries at each cell, the correlation coefficients  
186        identified from each cell to the observed reference (1990–2017) are applied  
187        to the projected reference. This is tenable since the timeseries are dom-  
188        inated by the yearly hydrologic cycle, and, the flat topography results in  
189        high correlations between model cell hydrologic response as noted above.  
190        These projections are purely probabilistic, and do not account for climate  
191        change or nonstationarity.

### 192        2.5. *Sea Level Rise Data*

193        Sea level rise trajectories applied to the future projection model are ob-  
194        tained from Park et al. (2017) corresponding to low (50<sup>th</sup> percentile) and  
195        high (99<sup>th</sup> percentile) estimates from 2015 through 2100. These estimates  
196        are specific to South Florida, and based on a synthesis of tide gauge data,  
197        global climate models and expert elicitation, contributions from the Green-  
198        land ice sheet, West Antarctic ice sheet, East Antarctic ice sheet, glaciers,  
199        thermal expansion, regional ocean dynamics, land water storage and long-  
200        term, local, non-climatic factors, such as glacial isostatic adjustment, sedi-  
201        ment compaction and tectonics.

202        As noted in Park et al. (2017), these projections are comprehensive, but  
203        do not include components related to a rapid collapse of Greenland and  
204        Antarctic ice sheets. Recent observations suggest that such a collapse is  
205        underway (Holland et al., 2015; Wouters et al., 2015), thereby we select the  
206        median projection as the low, and the 99<sup>th</sup> percentile as the high. The sea  
207        level rise projections and projected marsh water levels are shown in figure  
208        4.

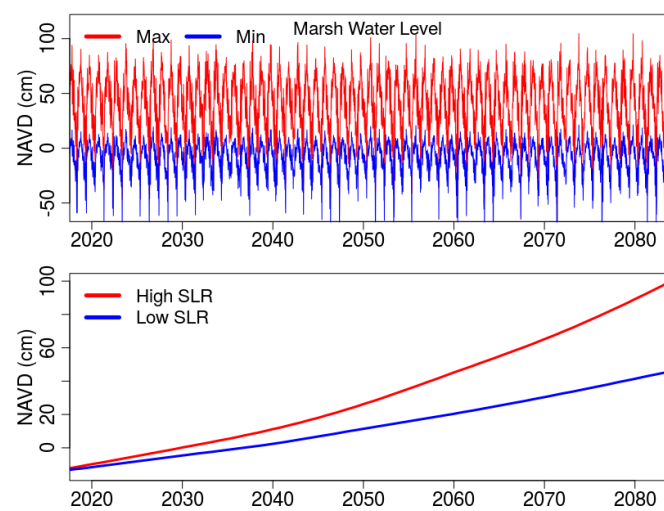


Figure 4: Sea level rise projections (bottom) and projected minimum and maximum marsh water levels (top). Elevations are National Vertical Datum of 1988 (NAVD 88).

209    2.6. Calibration Model

210    Calibration of agent thresholds and behaviors is achieved by initializing  
 211    a model spanning the current mangrove/sawgrass ecotone with vegetation  
 212    coverage observed in 1973 (Rintz and Loope, 1978), which at the time was  
 213    a purely freshwater landscape as shown in figure 5a). The model domain is  
 214    a grid of 22,990 patches (209 x 110) covering a spatial domain of 10,450 x  
 215    5,500 m. However, only 17,680 patches are used according to the extent of  
 216    the 1973 vegetation map.

217    The model is a four-species model with three freshwater species account-  
 218    ing for 98.8% of the initial vegetation (Sawgrass 92.0%, Spikerush 4.3%, Wax  
 219    Myrtle 2.5%), and Red mangrove as the saline successor. Other species com-  
 220    prising 1.2% of the initial vegetation are not processed. The model is run  
 221    forward in time from 1973 to 2015 with parameters adjusted to best fit the  
 222    observed 2015 landscape vegetation (figure 5b). Fit is defined as the per-  
 223    centage of model patches that correspond to the 2015 observed vegetation  
 224    at the end of the model run. An example applied to two model parameters  
 225    is shown in figure B.13 of Appendix B.

226    Sea level rise is modeled as a linear function increasing at 3 cm/decade,  
 227    corresponding to the mean of observed linear trends at Vaca Key (3.69  
 228    mm/yr) and Key West (2.42 mm/yr).

229    Model output is shown in figure 5c. Model parameters are listed in

230 Appendix B, model code and data are available at  
231 <https://github.com/SoftwareLiteracyFoundation/Ecotone>.

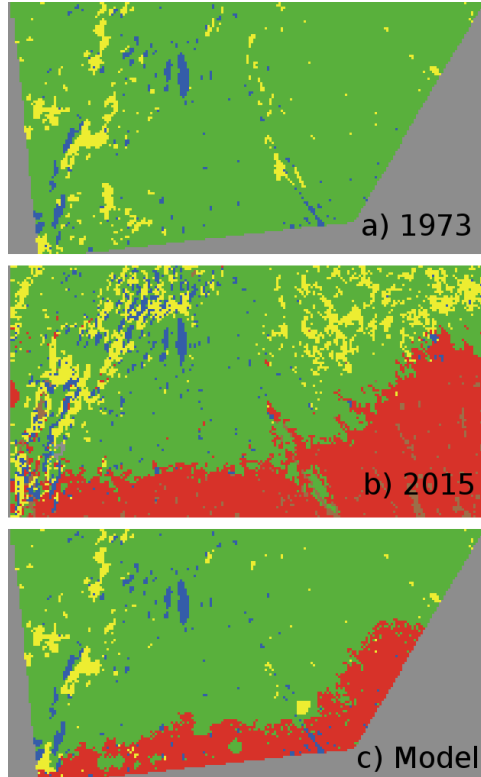


Figure 5: a) Initial vegetation, 1973. b) Final vegetation, 2015. c) Calibration model output at 2015.

### 232 2.7. Projection Model

233 The projection model is a spatial expansion of the calibration model with  
234 vegetation initialized from the 2015 vegetation map where available, and  
235 with timeseries of marsh stage and sea levels projected from 2015 to 2100.  
236 The spatial domain is expanded by 8.6 km to the north and initialized with  
237 sawgrass since there is not a vegetation map in this region. The resultant  
238 model domain covers 14,382 hectare in a grid of 57,528 patches (204 x 282)  
239 10.2 km wide by 14.1 km tall along the fresh to saline ecotone near Taylor  
240 Slough, Everglades National Park (figure 2).

241 The model uses parameters determined by the calibration model (table  
242 B.11), with the addition of one parameter: `msl-open-depth` and three vege-

tation species, Cypress, Swamp Bay and Buttonwood. The `msl-open-depth` defines a patch depth that when exceeded by mean sea level converts the patch from terrestrial to marine/estuarine. It is set to 70 cm corresponding to maximal freshwater depths.

The three additional species account for 3.5% of the initial species coverage and not considered for propagation. They are assessed for vitality and can die in response to either MSL exceeding the patch elevation plus `msl-open-depth`, or to salinity exposure in the case of Cypress and Swamp Bay. Their salinity thresholds are set to a maximum salinity of 1 ppt sustained over a period of 30 days.

Model code and data are available at  
<https://github.com/SoftwareLiteracyFoundation/Ecotone>.

### 3. Results

Predicted landscape transformations under low and high sea level rise trajectories are shown in figures 6 and 7 respectively. Under the low sea level rise projection the landscape is relatively unchanged through 2050, with the emergence of a mangrove stand in the south-central model domain. By 2060, the mangrove stand has expanded, and by 2070 it has nearly engulfed the slightly elevated ridge running from the south central of the domain to the northeast. Landscape elevations are shown in Appendix A.6.1. By 2080 the majority of the landscape seaward of the porewater salinity interface has transformed to mangroves, with the emergence of an open water area in the southwest corner of the domain.

In response to the high sea level rise trajectory, significant change is not forecast through 2040, with the emergence of the south-central mangrove stand by 2050. The ensuing decade is forecast to support the rapid colonization of mangroves along the slightly elevated ridge. By 2070, there has been substantial transformation with open water accounting for a major portion of the domain and a new coastline of mangrove swamp. By 2080 the transformation from predominantly freshwater marsh to marine conditions and mangrove swamp is nearly complete.

Quantification of the areal change in landscape dominant species vegetation cover in response to the two sea level rise forcings is shown in figure 8. Under both scenarios the contemporary vegetation distributions remain in equilibrium until 2050, beyond which there is evidence of landscape transformation from freshwater marsh to mangrove marsh and open water.

The physical mechanism behind freshwater to saline-tolerant vegetation transformation is infiltration of root zone porewater salinity. It is also known

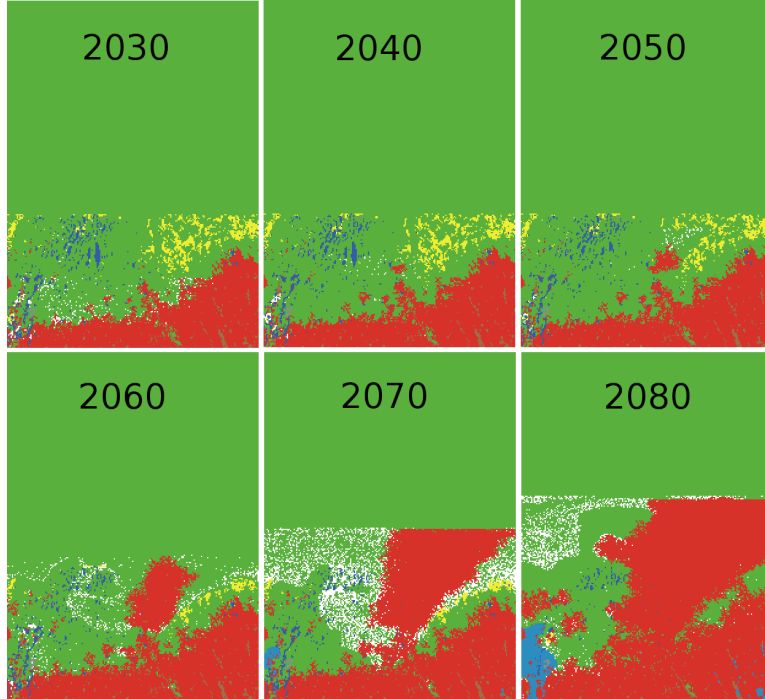


Figure 6: Projected vegetation transformation in response to a low sea level rise trajectory. Vegetation colors correspond to the legend in figure 2. White indicates a dead patch.

that as saline water from rising ocean levels infiltrate landward in the surficial aquifer, it does so from the “bottom-up” since saline water is denser than the freshwater (Dausman and Langevin, 2005). From this, we assume that at a point on the landscape where freshwater vegetation has been displaced that the saline water extends to the base of the surficial aquifer.

Given estimates of the surficial aquifer thickness, which here range from approximately 8 to 12 m (Causaras, 1986), and which are spatially mapped in the model GIS coverage, one can make conservative estimates of the freshwater volume replaced by saline water by using the vegetation coverage as an ecosystem response function. Figure 9 plots estimates of surficial aquifer volumes under the model domain of fresh and saline water in response to the two sea level rise trajectories assuming a porewater volume fraction of 0.2 (Dausman and Langevin, 2005). Note that this does not require detailed estimates of aquifer properties such as hydraulic conductivity, and that it is not required to estimate landscape vegetation changes.

Model results indicate a transformation from current ecological equilib-

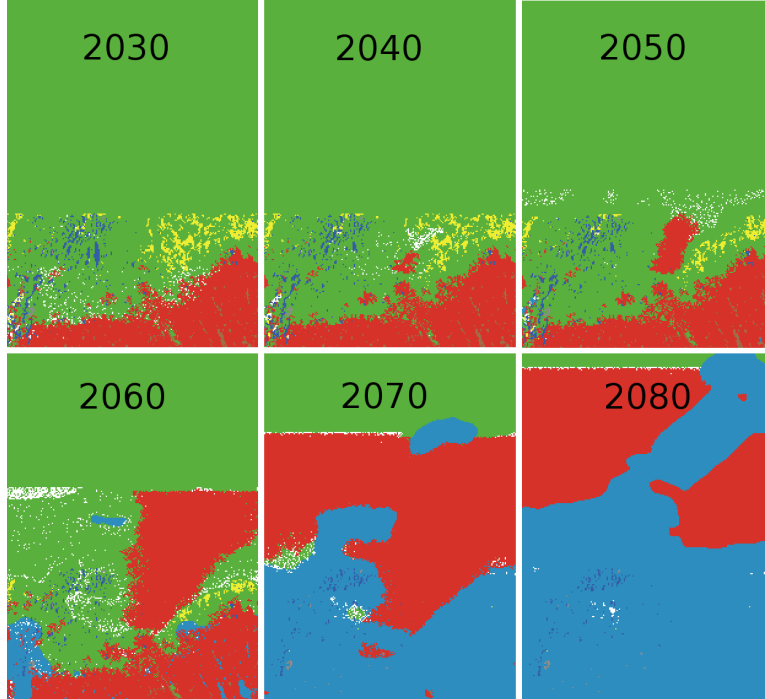


Figure 7: Projected vegetation transformation in response to a high sea level rise trajectory. Vegetation colors correspond to the legend in figure 2. White indicates a dead patch.

rium to saltwater dominated starting at 2050. Dynamics of this transition from the freshwater biome perspective are presented in figure 10 where deviation of spatially-averaged projected freshwater levels on land are compared with coverage of the dominant freshwater species from 2050 through 2070. Here, we find dynamic responses at two timescales. The long-term decline driven by increasing porewater salinity as ocean levels rise, superimposed with shorter-term yearly or interannual variations exhibiting species proliferation and recovery, with punctuated events of rapid species decline. The rapid declines appear well-correlated with low freshwater elevation events, consistent with observations that drought and dry conditions are a fundamental stressor of freshwater marsh plants, while recovery is indicated during periods without deep water level recession (2054–2058).

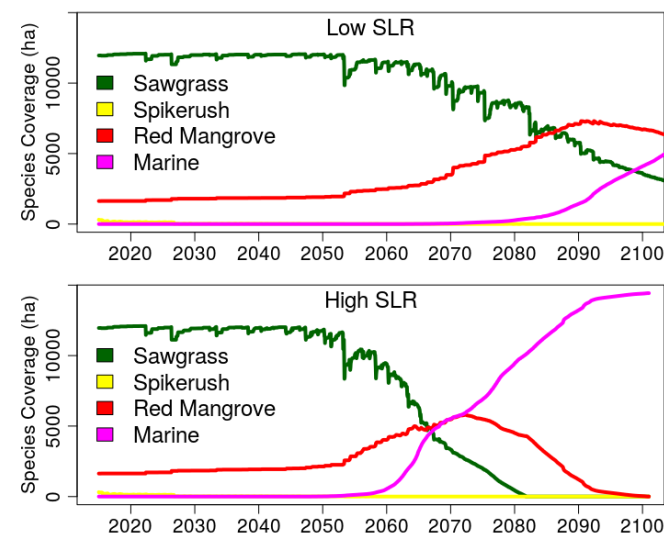


Figure 8: Projection of dominant vegetation coverage and marine (open) area for the low (top) and high (bottom) sea level rise trajectories.

#### 310 4. Discussion

310 Following the suggestion of Sivapalan (2018) that complex eco-hydrologic  
 311 domains can be assessed through ecosystem function expressed on the land-  
 312 scape, and the recognition of Jiang et al. (2016) that linear, correlation-  
 313 based models may not be ideal for capturing ecotone dynamics, we find  
 314 that an agent based model provides reasonable and compelling estimates  
 315 for landscape and freshwater resource transformation of coastal marshes in  
 316 response to sea level rise. The agent based approach relies on specifica-  
 317 tion of interactions between the environment and species competing on the  
 318 landscape, rather than highly detailed mappings and assumptions of sub-  
 319 terranean aquifer geology and environmental forcings such as rainfall and  
 320 evapotranspiration. If we were not interested in quantifying the aquifer  
 321 resource transformation, but simply inferring it's areal coverage from the  
 322 vegetative landscape response, we would not need geologic properties at all.

323 The model exhibits interspecies competition between fresh and saline  
 324 tolerant plants, primarily sawgrass (*Cladium jamaicense*) and red mangrove  
 325 (*Rhizophora mangle*), mediated by root zone porewater salinity determined  
 326 by elevations of rain-supplied marsh water level, land surface, and sea level.  
 327 Consistent with known landscape response, elevated porewater salinity de-  
 328 natures freshwater plants during periods of low marsh water level. Open

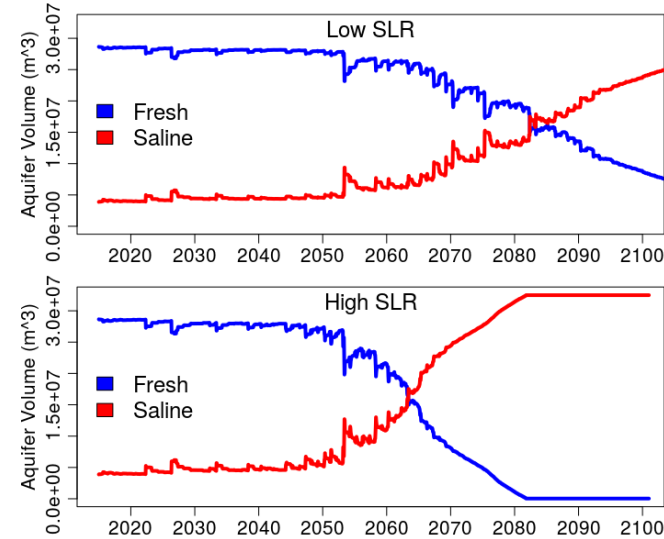


Figure 9: Projection of Fresh and saline water aquifer volumes under the model domain for the low (top) and high (bottom) sea level rise trajectories.

329 patches are then colonized with fresh or salt tolerant plants depending on  
330 environmentally determined fitness functions of surrounding species.

331 Model results predict continued equilibrium between fresh and saltwater  
332 species until 2050, after which there is eventual replacement of freshwater  
333 species with salt tolerant ones and fresh groundwater with saline groundwater,  
334 ultimately transitioning into new marine habitat. Interestingly, initiation  
335 of the transformation is essentially independent of whether sea levels  
336 rise along a low or high trajectory, however, the ensuing transformations  
337 are quite different as a function of sea level dynamics. This likely reflects  
338 a difference between the low and high sea level rise trajectories of 13 cm  
339 between 2020 and 2050, but 70 cm between 2050 and 2100. Under a low sea  
340 level rise trajectory the model domain transitions from freshwater resource  
341 volume of 28.6 million cubic meters in 2015 to 8.7 million cubic meters in  
342 2100, while under a high trajectory the volume decreases to 0 by 2085.

343 The model also predicts that mangrove establishment at the 2050 thresh-  
344 old is facilitated along a slightly elevated ridge that runs northeast from the  
345 lower central model domain. This elevation difference is no more than 14  
346 cm above the surrounding marsh.

347 The anticipated landscape and aquifer transformation horizons of 2050–  
348 2070 are consistent with a purely empirical, independent mechanism and

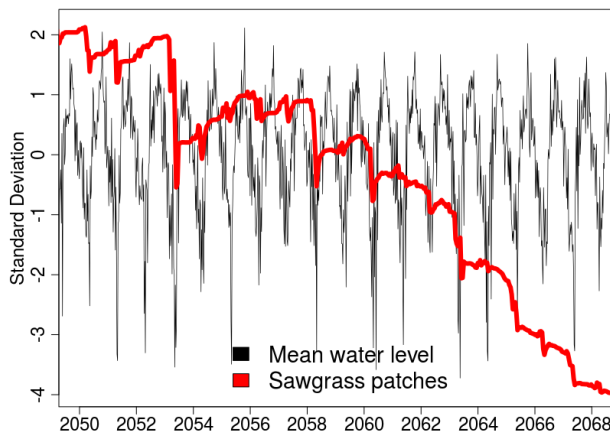


Figure 10: Deviation of spatially-averaged marsh projected water levels compared to scaled sawgrass patch count. Rapid declines in species coverage appear well-correlated with low freshwater elevation events.

analysis by Park et al. (2017a) assessing transformations in water level exceedances along the coastal ridge in Florida Bay, 8.5 km directly south and seaward of the current mangrove-freshwater ecotone. There, the transformation horizon of 2040–2070 is forecast for the coastal ridge to be continually inundated in response to the same sea level rise trajectories.

As sea level rises, Florida Bay will expand into the Everglades and South Florida establishing new estuarine and marine habitats replacing fresh groundwater along the coastal ecotone. The model predicts that avoidance of extreme low water events and generally higher marsh stage are keys to prolonging viability of freshwater resources, goals expressed in the Comprehensive Everglades Restoration Plan (NAS, 2018).

Further, as shown in the upper right of figure 2 and lower right of figure 1, the South-Dade agricultural areas are less than 10 km from the model domain. This industry employs more than 20,000 people producing more than \$2.7 billion in annual economic impact (Miami Dade Co., 2019), and is predicated on the surficial aquifer as a source of freshwater. Additionally, the Florida Keys Aquaduct Authority extracts potable water for over 70,000 residents from a wellfield located less than 5 km from the southern boundary of the agricultural area providing significant concern for saline intrusion (McThenia et al., 2017). Our results suggest that near the end of the century, these areas can start experiencing freshwater resource reduction.

Finally, we note that the model is based on species-specific behaviors in response to root zone porewater salinity with freshwater graminoids and red

<sup>372</sup> mangroves the dominant cross–ecotone species. Similar coastal ecotones are  
<sup>373</sup> found around the globe and can be assessed for water resource transforma-  
<sup>374</sup> tions using these methods.

375 **Appendix A. Model Overview, Design concepts, and Details (ODD)**

376 *Appendix A.1. Purpose*

377 The models dynamically quantify areal transformation of freshwater  
378 marsh into saline estuary in response to dynamic interactions between fresh-  
379 water depth and root zone porewater salinity driven by sea level. Landscape  
380 vegetation changes are used as indicators of surficial groundwater saliniza-  
381 tion, allowing estimates of changes fresh-to-saline water volumes in the  
382 surficial aquifer.

383 *Appendix A.2. Entities, state variables, and scales*

384 *Appendix A.2.1. Agents*

385 Model agents consist of plant species (NetLogo turtles) and landscape  
386 grid cells (NetLogo patches). Plant species agents are listed in table A.1  
387 with initial coverage percentages listed in tables A.8 and A.9. The Open  
388 Water agent is an end-point transformation for the other species.

389 State variables of the plant and grid cell agents are listed in tables A.2  
390 and A.3 respectively.

391 *Appendix A.2.2. Spatial units*

392 Landscape grid cells correspond to the 50m x 50m spatial discretisation  
393 of the vegetation map developed by Ruiz et al. (2017).

394 The calibration model domain is a grid of 22,990 patches (209 x 110)  
395 covering a spatial domain of 10.4 x 5.5 km. The projection model covers  
396 14,382 hectare in a grid of 57,528 patches (204 x 282) 10.2 km wide by 14.1  
397 km tall.

Table A.1: Model Agents.

Species	Calibration Model	Projection Model
Red Mangrove	X	X
Sawgrass	X	X
Spikerush	X	X
Buttonwood		X
Cypress		X
Swamp Bay		X
Wax Myrtle	X	
Open Water	X	X

Table A.2: Plant species variables.

Variable	Unit	Description
<code>species</code>		Species name
<code>salinity_max</code>	ppt	Maximum tolerable salinity
<code>salinity_max_days</code>	days	Maximum duration of tolerable salinity

Table A.3: Landscape cell variables.

Variable	Unit	Description
<code>depth</code>	cm	Water depth
<code>days_wet</code>	days	Hydroperiod
<code>days_dry</code>	days	Consecutive days dry land surface
<code>salinity</code>	ppt	Salinity from timeseries (optional)
<code>porewater_salinity</code>	ppt	Root zone porewater salinity
<code>salinity_threshold</code>	ppt	Salinity the current cell species can tolerate
<code>salinity_days</code>	days	Consecutive days with salinity above threshold
<code>cell_ID</code>		Cell ID from vegetation map
<code>elevation</code>	cm	Ground elevation (NAVD88)
<code>reason_died</code>		Reason species died
<code>day_died</code>	date	Date the species died
<code>stage_gauge</code>		Gauge for water stage timeseries
<code>aquifer_m</code>	m	Aquifer thickness
<code>species_init</code>		Initial species

398     *Appendix A.2.3. Environment*

399     The model environment consists of three primary variables: land surface  
400     elevation, water depth in relation to land surface, and sea level elevation.  
401     Land surface elevation is assigned to each model grid cell from a GIS layer  
402     based on the work of Fennema et al. (2015) as described in section Appendix  
403     A.6.

404     Daily water elevations are obtained from the Everglades Depth Estima-  
405     tion Network (EDEN) (USGS, 2015) and mapped to landscape cells through  
406     a GIS layer and the cell `stage_gauge` variable. The GIS layer (specified  
407     in section Appendix A.6) assigns to each cell the name of an EDEN cell  
408     from which the water level timeseries are applied. A csv file of the EDEN  
409     timeseries data is dynamically accessed to retrieve the corresponding water  
410     elevation at each timestep.

411     Sea level elevations are obtained from timeseries of projected sea levels  
412     in Florida Bay by Park et al. (2017).

413     *Appendix A.3. Process overview and scheduling*

414     Model timesteps are discretely updated with a user-adjustable variable  
415     `days-per-tick` with a default value of 15 days. Since input data are avail-  
416     able in daily increments the model timestep can be any period of days.  
417     The appropriate data is selected according to the specific date of a model  
418     timestep.

419     The `go` function schedules agent and data process execution at each  
420     timestep as shown here and described in detail in Appendix A.7.

```
421       ; Load mean sea level for this timestep
422       set MSL time:ts-get MeanSeaLevel.data date SLR-scenario
423
424       update-patch-depth-salinity
425
426       ; Process species agentsets for environmental impact, vitality
427       go-sawgrass
428       go-spikerush
429       go-red-mangrove
430       go-cypress
431       go-swamp-bay
432       go-buttonwood
433
434       ; Process dead patches for succession
435       go-propagation
```

436  
437        tick ; increment time by days-per-tick

438        *Appendix A.4. Design concepts*

439        *Appendix A.4.1. Basic principles*

440        The models assume a fundamental driver of ecotone dynamics between  
441        freshwater marsh and saline estuary is root zone porewater salinity, and  
442        that this salinity is mediated by dynamic balance between sea level ele-  
443        vation, landscape cell elevation and freshwater that may be present on the  
444        cell. Species-specific tolerances to root zone salinity, hydroperiod and depth  
445        dictate plant vitality and death, while porewater salinity determines species-  
446        specific fitness for succession.

447        *Appendix A.4.2. Emergence*

448        The model is fundamentally one of interspecies competition driven by  
449        root zone salinity. Primal complexities arise from the nonlinear nature of  
450        landscape freshwater depth and randomness of plant death and succession.  
451        Therefore, we do not expect behavioral emergence from interagent interac-  
452        tions.

453        *Appendix A.4.3. Adaptation*

454        Vegetation agents do not internally adapt or change behaviors, but they  
455        do respond to environmental changes. These behaviors are governed by  
456        salinity thresholds prescribed by the logistic functions shown in figure 3,  
457        water depth and hydroperiod thresholds shown in table A.4, and succession  
458        probabilities listed in table A.5.

459        For example, based on observational data as expressed in Figure 3, saw-  
460        grass can tolerate salinities near 1 ppt while for spikerush 2 ppt can be  
461        tolerated. The depth parameter relates a water depth on the patch beyond  
462        which the plant is unable to transpire or its cellular structure is compro-  
463        mised, days wet represents the continuous hydroperiod that the plant can  
464        tolerate resulting in decomposition of roots, transpiration limits, or cellu-  
465        lar compromise. Days dry represents the tolerable period of time with no  
466        available water in the root zone resulting in desiccation.

467        Threshold and model parameters values are listed in table B.11 of Ap-  
468        pendix B.

469        As noted in section 2.2.2, when empty cells are evaluated for species  
470        succession the surrounding species with the highest cumulative fitness is  
471        selected for propagation. However, whether propagation actually occurs is  
472        determined by comparison of the species propagation success threshold as  
473        listed in table A.5 to a uniform random variate.

Table A.4: Vitality behaviors. When the condition variable exceeds the threshold, the plant dies. Thresholds are expressed as the NetLogo model variable name (table B.11).

Species	Condition
Red Mangrove	<code>MSL &gt; patch elevation + 80 cm</code>
Sawgrass	<code>depth &gt; sawgrass-depth-max</code>
Sawgrass	<code>days above salinity threshold &gt; sawgrass-salinity-threshold</code>
Spikerush	<code>depth &gt; spikerush-depth-max</code>
Spikerush	<code>days dry &gt; spikerush-days-dry</code>
Spikerush	<code>days above salinity threshold &gt; spikerush-salinity-threshold</code>
Wax Myrtle	<code>depth &gt; wax-myrtle-depth-max</code>
Wax Myrtle	<code>days wet &gt; wax-myrtle-days-wet</code>
Wax Myrtle	<code>days above salinity threshold &gt; wax-myrtle-salinity-threshold</code>

Table A.5: Succession failure conditions. Model parameter values are shown in table B.11.

Species	Condition
Sawgrass	<code>sawgrass-success &lt; uniform percentile</code>
Sawgrass	<code>depth &gt; sawgrass-depth-min</code>
Spikerush	<code>spikerush-success &lt; uniform percentile</code>
Spikerush	<code>days wet &lt; spikerush-days-wet</code>
Mangrove	<code>mangrove-success &lt; uniform percentile</code>
Mangrove	<code>depth &gt; depth-propagule</code>

474     *Appendix A.4.4. Objectives*

475       As noted in the preceding section, agents do not engage in internal behav-  
 476       ior or objective (fitness) adaptation, however, their objectives are responsive  
 477       to the environment as detailed in the preceding section.

478     *Appendix A.4.5. Learning*

479       As noted in the preceding section, agents do not alter or dynamically  
 480       change their adaptive traits, rather they respond to the environment.

481     *Appendix A.4.6. Prediction*

482       Agents do not project or anticipate future states.

483     *Appendix A.4.7. Sensing*

484       Environmental state variables that individuals are assumed to sense and  
 485       consider in their decisions are listed in table A.6.

486     *Appendix A.4.8. Interaction*

487       Interactions exist between the landscape cell (NetLogo patch) and the  
 488       vegetation agent (NetLogo turtle) on the cell. The cell maintains informa-

Table A.6: Plant species agent environmental sensing variables.

Species	Variable	Description
Sawgrass	MSL	Mean sea level elevation
	depth	Landscape water depth
	days_wet	Consecutive days with inundation
	salinity_days	Consecutive days above salinity threshold
Spikerush	days_dry	Consecutive days without inundation
	salinity_days	Consecutive days above salinity threshold
Red Mangrove	MSL	Mean sea level elevation
	MSL	Mean sea level elevation
	salinity_days	Consecutive days above salinity threshold
Cypress	MSL	Mean sea level elevation
Swamp Bay	salinity_days	Consecutive days above salinity threshold
	MSL	Mean sea level elevation
	salinity_days	Consecutive days above salinity threshold
Buttonwood	MSL	Mean sea level elevation
	MSL	Mean sea level elevation
Wax Myrtle	days_wet	Consecutive days with inundation
	depth	Landscape water depth

Table A.7: Hydroperiod modulation.

Species	Variable	Min	Max	Modulation
Sawgrass	days-wet	0	365	$N(0,15)$ days
Wax Myrtle	days-wet	0	1000	$N(0,15)$ days
Spikerush	days-dry	0	1000	$N(0,10)$ days

489 tion regarding water depth, hydroperiod, and porewater salinity. Vegetation  
 490 agents process this state information to determine vitality and fitness. There  
 491 are no interagent interactions between vegetation agents.

492 The only feedback in the model acts within landscape cells to determine  
 493 porewater salinity. Porewater salinity is forced by the elevation of mean sea  
 494 level in relation to the elevation of the cell (land surface), but can be medi-  
 495 ated by the presence of adequate freshwater depth on the cell as described  
 496 in Appendix A.7.1.

#### 497 *Appendix A.4.9. Stochasticity*

498 Evaluation of environmental variables **days-wet** and **days-dry** in plant  
 499 vitality behaviors are randomly modulated with a Gaussian kernel to sim-  
 500 ulate individual plant tolerances. Specifically, when a patch hydroperiod is  
 501 processed, the physically simulated value is shifted by the number of days  
 502 according to a normal distribution specified in table A.7.

503 Vegetation succession behaviors are also probabilistically influenced as  
 504 described in section 2.2.2 and Appendix A.4.3.

Table A.8: Initial species of the calibration model.

Species	Count	Percent
Sawgrass	16256	92.0
Spikerush	758	4.3
Wax Myrtle	441	2.5
Cypress	125	0.7
Red Mangrove	0	0.0

Table A.9: Initial species of the projection model.

Species	Count	Percent
Sawgrass	47835	83.1
Red Mangrove	6523	11.3
Spikerush	1258	2.1
Cypress	1070	1.8
Swamp Bay	671	1.1
Buttonwood	395	0.6

505 *Appendix A.4.10. Collectives*

506 The models use agent collectives (NetLogo agentsets) internally to avoid  
 507 redundant operations. For example, collectives of cells with specific species,  
 508 or which have transformed to open water. There are no collective behaviors  
 509 associated with these collectives.

510 *Appendix A.4.11. Observation*

511 The number of patches of sawgrass and red mangrove are the primary  
 512 observational variables of the models.

513 *Appendix A.5. Initialization*

514 Each cell in the model is initialized with a vegetation species specified  
 515 from a vegetation map. The calibration model uses the 1973 vegetation map  
 516 of Rintz and Loope (1978), while the prediction model uses the 2015 map  
 517 of Ruiz et al. (2017). Timeseries data of water depth and mean sea level  
 518 elevation are initialized according to the user-specified `start-date` variable.  
 519 Section Appendix A.6 details the input and initialization data.

520 Initial species compositions for the calibration and projection models are  
 521 shown in tables A.8 and A.9 respectively.

522 *Appendix A.6. Input data*

523 Table A.10 lists the input files and associated variable names used in  
 524 the models. All timeseries data have daily resolution, and extend over the  
 525 model period of record with no repeated data.

Table A.10: Data input files.

Model Variable	File type	Purpose
<b>Stage.data</b>	csv	Marsh water level
<b>MeanSeaLevel.data</b>	csv	Mean sea level
<b>VegMap</b>	shp	Species to cell mapping, cell elevation
<b>GaugeZones</b>	shp	EDEN data to cell mapping

526 Sea level rise and marsh water level extrema are shown in figure 4, cell  
 527 elevations are shown in figure A.11.

528 *Appendix A.6.1. Elevation Data*

529 The interplay between freshwater depths, mean sea level and porewater  
 530 salinity are largely determined by landscape elevation. Figure A.11 shows  
 531 the model domain elevation indicating a southwest to northeast channel  
 532 known locally as Taylor Slough. There is also a small ridge south of Taylor  
 533 Slough running southwest to northeast. Model simulations suggest that this  
 534 ridge will provide an initial stand for red mangroves as sea levels rise.

535

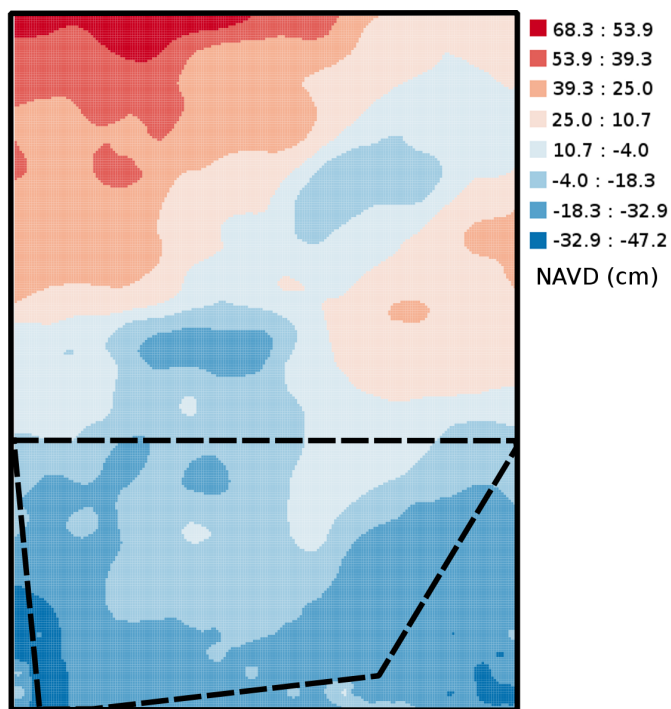


Figure A.11: Elevation map of the model domain. Dashed polygon is the calibration model domain.

536 *Appendix A.6.2. Aquifer Geological Data*

537 Aquifer thickness is inferred from United States Geological Service wells  
 538 and geologic cross-sections shown in figure A.12.

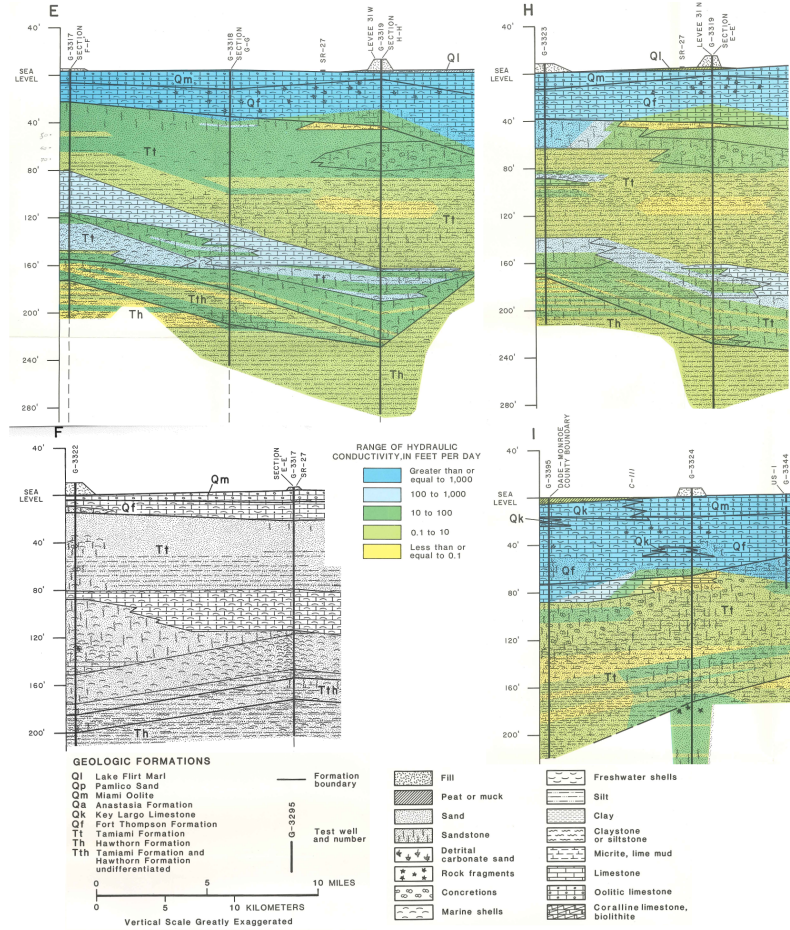


Figure A.12: Geologic cross sections from United States Geological Service wells (Causaras, 1986)

539 *Appendix A.7. Submodels*

540 Model processes specified in Appendix A.3 are detailed here.

541     *Appendix A.7.1. Update Patch Depth Salinity*

542       The procedure `update-patch-depth-salinity` executes these steps at  
543       each timestep:

- 544       1. Set depth on all cells.
- 545       2. Accumulate hydroperiod (`days_wet`, `days_dry`) for all cells.
- 546       3. Identify cells with elevation below mean sea level into `msl_patches`.
- 547       4. Identify `msl_patches` in coastal zone within 1.5 km of mangrove eco-  
548       tone.
- 549       5. Identify `msl_patches` cells with freshwater depth less than `depth-no-porewater`  
550       into `porewater_patches`.
- 551       6. Increment `porewater_salinity` of `porewater_patches`.
- 552       7. Identify `msl_patches` with freshwater depth greater than `depth-no-porewater`  
553       into `no_porewater_patches`.
- 554       8. Reset `porewater_salinity` to zero for `no_porewater_patches`.
- 555       9. For `msl_patches`:
  - 556           (a) Update cell salinity.
  - 557           (b) Accumulate number of days above `salinity_threshold` into `salinity_days`.

558     *Appendix A.7.2. Plant Vitalities*

559       Each plant species/agent is assessed for vitality based on the current  
560       and accumulated environmental conditions in the `go-species` procedures.  
561       These procedures follow a common set of steps based on the the specific  
562       tolerances for each species as identified in Appendix A.4.3.

- 563       1. Identify cells with living species (i.e. sawgrass).
- 564       2. If needed, apply Gaussian offsets to hydroperiod variables to emulate  
565       individual plant tolerances as described in Appendix A.4.9.
- 566       3. Determine if the plants die by applying the environmental conditions  
567       and species thresholds described in Appendix A.4.3.
- 568       4. If plant has died, record the model time and reason for death.
- 569       5. If plant has died, remove the cell from the species cell collection.

570     *Appendix A.7.3. Succession*

571       The `go-propagation` procedure processes patches with no living plants  
572       for succession.

- 573       1. Identify species on surrounding (8) cells into `neighbor_species`.
- 574       2. Accumulate the porewater salinity mediated fitness score (figure 3) for  
575       each species in `neighbor_species`.

- 576     3. If there is a tie in fitness, randomly (50% uniform deviate) select one  
577       of the species and reduce its fitness by 0.1.  
578     4. Identify the species with maximum cumulative fitness.  
579     5. Apply the species-specific propagation threshold against a uniform  
580       random variate to decide if the selected species will actually propagate  
581       as described in section 2.2.2.  
582     6. If a species establishes on the cell, set the species-specific environmen-  
583       tal tolerances into the cell agent variables.

584    **Appendix B. Calibration Model**

585    Calibration model parameters are shown in table B.11.

Table B.11: Calibration Model Parameters

Parameter	Value	Description
msl-offset	2 cm	Elevation below Mean Sea Level
depth-no-porewater	2 cm	Marsh water depth min for fresh root zone
mangrove-success	33%	Probability of propagation success
depth-propagule	7 cm	Maximum depth for propagule establishment
sawgrass-success	33%	Probability of propagation success
sawgrass-depth-min	20 cm	Maximum depth for propagation
sawgrass-depth-max	180 cm	Maximum depth for survival
sawgrass-salinity-threshold	1	Salinity threshold for survival
sawgrass-salt-days	20	Maximum number of days above threshold
spikerush-success	33%	Probability of propagation success
spikerush-days-wet	730	Hydroperiod for propagation
spikerush-depth-max	80 cm	Maximum depth for survival
spikerush-days-dry	170 cm	Maximum days dry for survival
spikerush-salinity-threshold	2	Salinity threshold for survival
spikerush-salt-days	20	Maximum number of days above threshold
wax-myrtle-depth-max	180 cm	Maximum depth for survival
wax-myrtle-days-wet	370	Maximum hydroperiod for survival

586     Figure B.13 plots model calibration fit in response to `msl-offset` and  
587     `depth-no-porewater` finding optimal values of 2 cm for both parameters.  
588     Fit is defined as the percentage of model patches that correspond to the  
589     2015 observed vegetation at the end of the model run.

590

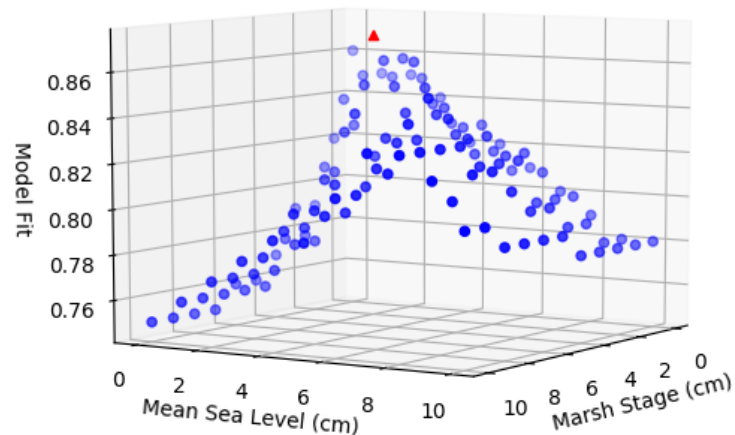


Figure B.13: Model fit as a function of mean sea level offset and marsh stage offset that control porewater salinity.

591        The NetLogo user interface for the calibration model is shown in figure  
 592        B.14.

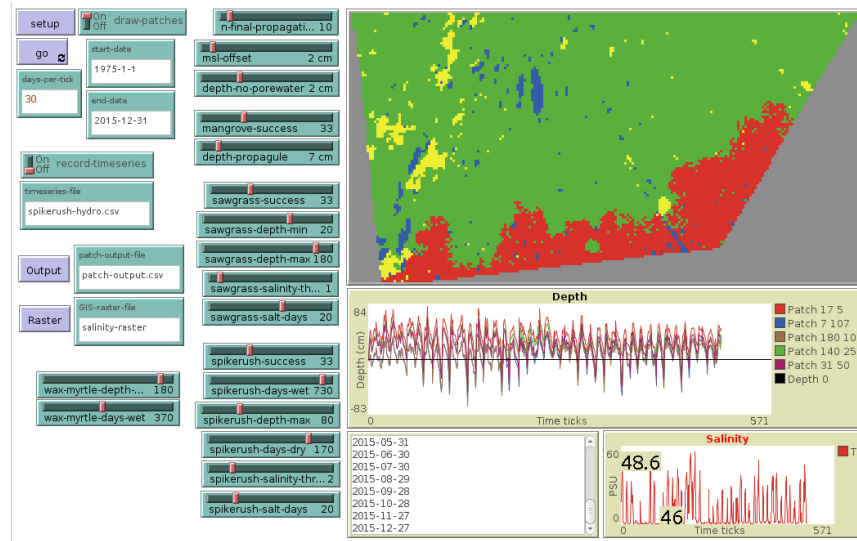


Figure B.14: NetLogo model user interface for the calibration model.

593 **Appendix C. Projection Model**

594 The projection model uses the same parameters as the Calibration model  
 595 (table B.11). The NetLogo user interface for the projection model is shown  
 596 in figure C.15.

597

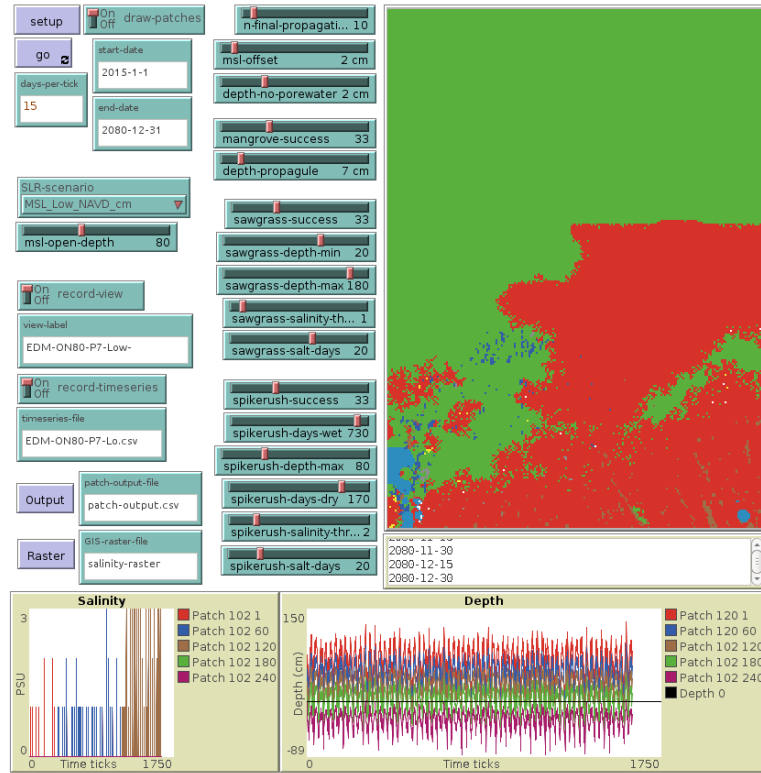


Figure C.15: NetLogo model user interface for the projection model.

598 **Appendix D. Aquifer Volume Fit**

599 A generalized logistic function  $V = V_0 + \frac{V_{max}}{1+exp(-a(x-x_0))}$  is fit to the  
 600 aquifer volume estimates with a Nelder-Mead optimization (Nelder and  
 601 Mead, 1965) as shown in figure D.16 and table D.12.

602

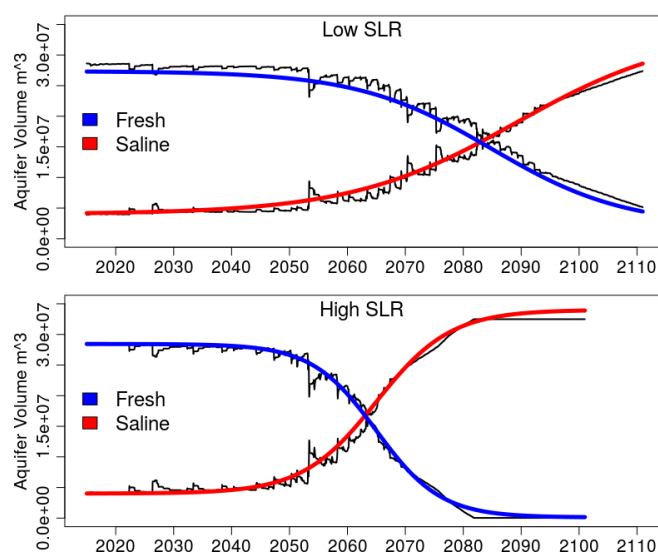


Figure D.16: Generalized logistic function fits to the estimated aquifer water volumes.

Table D.12: Best fit parameters for generalized logistic function  $V = V_0 + \frac{V_{max}}{1+exp(-a(x-x_0))}$  fit to estimated aquifer water volumes.

SLR	Water	a	$V_{max}$	$V_0$	$x_0$
Low	Salt	0.0001907	29999684	4011159	2089-04-04
Low	Fresh	-0.0002369	25303766	2051779	2084-11-14
High	Salt	0.0004285	29999999	4010603	2064-12-31
High	Fresh	-0.0004918	28322591	117512	2064-12-31

603    **References**

- 604    Causaras, C. A. (1986). Geology of the surficial aquifer system, Dade County,  
605    Florida, Water-Resources Investigations Report 86-4126, U.S. Geological  
606    Survey, doi:10.3133/wri864126.
- 607    Dausman, A., and Langevin, C.D., (2005). Movement of the saltwater in-  
608    terface in the surficial aquifer system in response to hydrologic stresses  
609    and water-management practices, Broward County, Florida. USGS Sci-  
610    entific Investigations Report 2004-5256. [http://pubs.usgs.gov/sir/](http://pubs.usgs.gov/sir/2004/5256/)  
611    2004/5256/
- 612    DeAngelis D.L., Yurek S. (2015). Equation-free modeling unravels the  
613    behavior of complex ecological systems. PNAS 112 (13) 3856-3857,  
614    doi:10.1073/pnas.1503154112.
- 615    Fennema, R., James, F., Bhatt, T., Mullins, T., Alarcon, C. (2015). EVER  
616    Elevation (version 1): A multi-sourced Digital Elevation Model for Ever-  
617    glades National Park. National Park Service, Everglades National Park,  
618    950 N Krome Ave. Homestead FL, USA, July 10, 2015.
- 619    Grimm V., Railsback S.F. (2005). *Individual-Based Modeling and Ecology*,  
620    Princeton Univ Press, Princeton, NJ.
- 621    Grimm V., Berger U., DeAngelis D., Polhill J., Giske J., Railsback F. (2010).  
622    The ODD protocol: A review and first update. Ecological Modelling 221,  
623    27602768. doi:10.1016/j.ecolmodel.2010.08.019.
- 624    Holland, P. R., A. Brisbourne, H. F. J. Corr, D. McGrath, K. Purdon, J.  
625    Paden, H. A. Fricker, F. S. Paolo, and A. H. Fleming (2015). Oceanic and  
626    atmospheric forcing of Larsen C Ice-Shelf thinning, The Cryosurgery, 9,  
627    1005-1024, doi:10.5194/tc-9-1005-2015.
- 628    Jiang J, DeAngelis D., Teh S., Krauss K., Wang H., Lie H., Smith T.,  
629    Koh H., (2016). Defining the next generation modeling of coastal ecotone  
630    dynamics in response to global change. Ecological Modelling, 326, 24 April  
631    2016, 168-176. <https://doi.org/10.1016/j.ecolmodel.2015.04.013>.
- 632    Jorgensen, S. E. (1996). *Handbook of environmental and ecological modeling*.  
633    CRC Press. Boca Raton, FL. 688 p., ISBN 978-1-56670-202-7.
- 634    Miami-Dade County Agriculture, (2019). <https://www.miamidade.gov/business/agriculture.asp>. Accessed January 3, 2019.

- 636 McThenia A., Martin W., and J Reynolds, (2017). Rising Tides  
637 and Sinking Brines: Managing the Threat of Salt Water In-  
638 trusion. Florida Water Resources Journal, August, 32–38.  
639 <https://fkaa.blob.core.windows.net/linkdocs/Managing%20the%20Threat%20of%20Salt%20Water%20Intrusion.pdf>.
- 641 National Academies of Sciences, Engineering, and Medicine (2018). Progress  
642 Toward Restoring the Everglades: The Seventh Biennial Review - 2018.  
643 Washington, DC: The National Academies Press. 210 p. ISBN: 978-0-309-  
644 47978-3 doi:10.17226/25198.
- 645 NASA Advisory Council. Earth System Sciences Committee. (1986).  
646 *Earth system science overview: a program for global change*. Wash-  
647 ington, D.C.: National Aeronautics and Space Administration, 50 p.,  
648 doi:10.17226/19210.
- 649 Nelder, J. A. and Mead, R. (1965). A simplex algorithm for function mini-  
650 mization. Computer Journal, 7, 308313. doi:10.1093/comjnl/7.4.308.
- 651 Park, J., Stabenau E., and K. Kotun (2017). Sea-level rise and in-  
652 undation scenarios for national parks in South Florida, Park Sci-  
653 ence 33(1):63-73. [https://www.nps.gov/articles/parkscience33-1\\_63-73\\_park\\_et\\_el\\_3860.htm](https://www.nps.gov/articles/parkscience33-1_63-73_park_et_el_3860.htm).
- 655 Park J., Stabenau E., Redwine J., Kotun K. (2017). South Florida's En-  
656 croachment of the Sea and Environmental Transformation over the 21st  
657 Century, J. Mar. Sci. Eng., 5(3), 31, doi:10.3390/jmse50300312017.
- 658 Rintz, R. E. and L. L. Loope (1978). Vegetation map of Taylor Slough,  
659 Everglades National Park, Florida. U.S. National Park Service, South  
660 Florida Research Center, Report T-566. Lyons Map Co. Miami, Florida.  
661 <http://purl.flvc.org/fcla/dt/3325304>.
- 662 Ross M., Meeder J., Sah J., Ruiz P. and G. Telesnicki (2000). The South-  
663 east Saline Everglades Revisited: 50 Years of Coastal Vegetation Change.  
664 Journal of Vegetation Science, 11(1), 101-112. <http://www.jstor.org/stable/3236781>.
- 666 Ruiz P., Giannini H., Prats M., Perry C., Foguer M., Garcia A., Sham-  
667 blin R., Whelan K., Hernandez M. (2017). The Everglades National  
668 Park and Big Cypress National Preserve Vegetation Mapping Project, In-  
669 terim Report Southeast Saline Everglades (Region 2). Everglades National

- 670 Park Natural Resource Report NPS/SFCN/NRR2017/1494. August 2017.  
671 <https://irma.nps.gov/DataStore/DownloadFile/583479>.
- 672 Schiff, Joel L. *Cellular Automata: A Discrete View of the World*. Wiley &  
673 Sons, Inc. ISBN 9781118030639. (2011).
- 674 Sivapalan, M. (2018). From engineering hydrology to Earth system science:  
675 milestones in the transformation of hydrologic science, *Hydrol. Earth Syst.*  
676 *Sci.*, 22, 1665-1693, doi:10.5194/hess-22-1665-2018.
- 677 Telis P.A., Zhixiao X., Zhongwei L., Yingru L, and Conrads P. (2015). The  
678 Everglades Depth Estimation Network (EDEN) Surface-Water Model,  
679 Version 2: U.S. Geological Survey Scientific Investigations Report 2014-  
680 5209, 42 p., doi 10.3133/sir20145209.
- 681 Wilensky, U. (1999). NetLogo. Center for Connected Learning and  
682 Computer-Based Modeling, Northwestern University, Evanston, IL. <http://ccl.northwestern.edu/netlogo/>.
- 684 Wouters B., A. Martin-Español, V. Helm, T. Flament, J. M. van Wessem, S.  
685 R. M. Ligtenberg, M. R. van den Broeke and J. L. Bamber (2015). Dy-  
686 namic thinning of glaciers on the Southern Antarctic Peninsula, *Science*,  
687 348 (6237) 899-903, doi:10.1126/science.aaa5727.